Vibration stabilization of a phase shifting interferometer for large optics

Glen C. Cole [a], James H. Burge [b], and Lee R. Dettmann [b]

[a] Eastman Kodak Company, 800 Lee Road, Rochester, N.Y. 14650
[b] Steward Observatory, University of Arizona, Tucson, Arizona 85721

ABSTRACT

Phase shifting interferometry requires an intentional shifting of the relative phase between the reference arm and the test arm of an interferometer. Vibration can lead to uncertainty in the relative phase difference with respect to time and result in erroneous surface measurements. We have developed a method for actively compensating for vibration using a closed-loop phase servo system. An essential feature of this is a high frequency phase measurement. The phase is modulated and the intensity variations are measured with a high speed photodiode and digitized. This information is processed by a DSP and a five step algorithm is used to determine the instantaneous phase. These high speed phase measurements are used in a closed loop phase servo to compensate for vibration and also allow for phase shifting interferometry. Test results with and without the vibration compensation device will be presented.

Keywords: phase shifting, interferometry, vibration, large optics, testing, metrology, telescopes

1. INTRODUCTION

Phase shifting interferometry is an increasingly powerful and useful tool in optical surface measurements. It allows for high accuracy, computer control and high spatial resolution. In phase shifting interferometry (PSI), intentional phase shifts are introduced between the reference and test arms of the interferometer. The intensities at these discrete phase values are used with simple algorithms to calculate the surface topography. Vibration can have a detrimental effect on PSI because the relative phase difference is not controlled as desired -- leading to errors in the surface maps.

This paper presents a novel solution to the problem of vibration with phase shifting interferometry. Our method uses a fast phase servo loop where the phase sample frequency is several kilo-Hertz. When a change is detected, the source frequency is shifted up or down in real time to compensate.

The hardware configuration duplicates the long test path of the Steward test tower and a PZT-driven (piezo-electric transducer) corner cube acts as a calibrated vibration source. The device was refined and tested on the optical table and the results are presented. Future improvements include reducing the minimum path lengths with the choice of the appropriate electro-optic element and expanding from a piston-only system to a piston-tip-tilt system.

2. METHOD DESCRIPTION

The device compensates for vibration with a closed-loop phase servo system. Figure 1 shows a block diagram of the servo. There are two external inputs to the system -- the command input (for surface measurements) and the external vibrations that must be compensated. The active element makes the servo correction.

SPIE Vol. 3134 • 0277-786X/97/$10.00

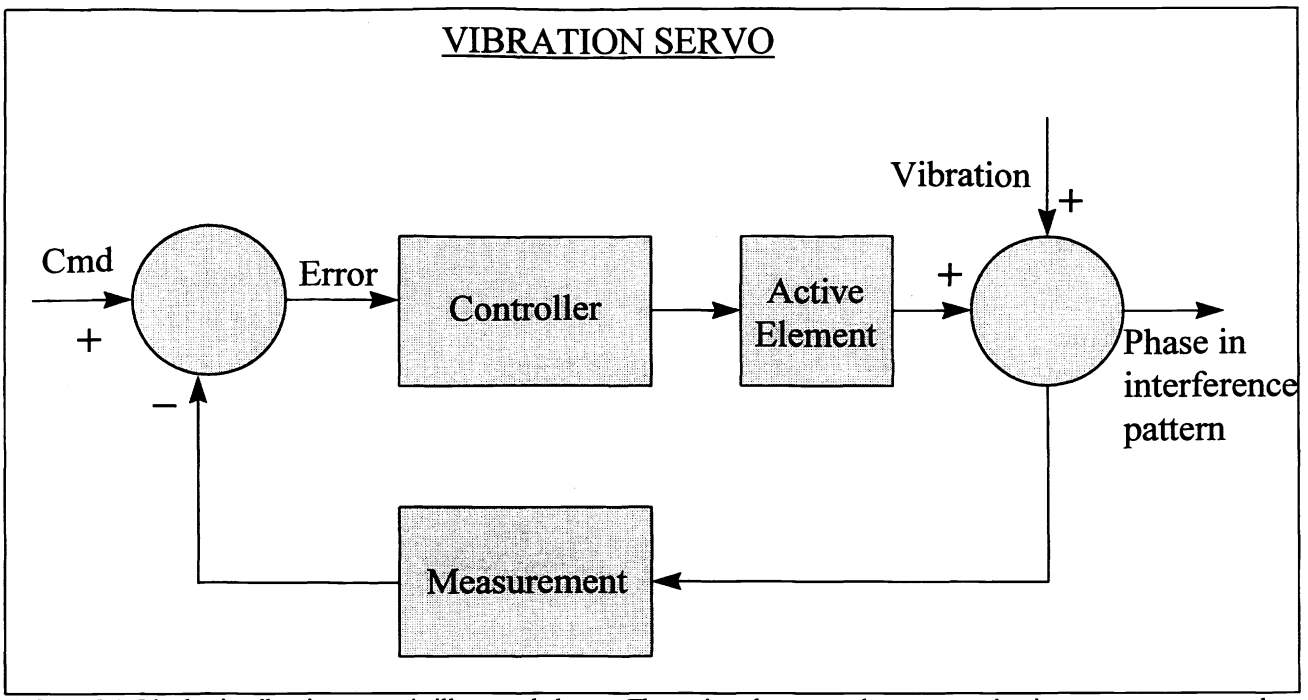

FIGURE 1. The basic vibration servo is illustrated above. The active element makes a correction in response to external inputs (from the surface map computer and vibration) to the system.

An essential feature of the method is a high frequency phase measurement. The details are shown in Figure 2. This servo measurement is made by quickly ramping the phase by 2π during which the intensity variations are measured with a high speed photodiode and digitized. This information is processed by a Digital Signal Processor or DSP and a five step algorithm is used to determine the instantaneous phase. Next, the phase is held constant followed by a rapid 2π shift in the opposite direction. In this way the system is measuring the phase at a sample frequency of 4000 Hertz.

These high speed phase measurements are used to close the vibration servo loop. If an error in phase is detected, a compensation is made. This is accomplished with the use of an Acousto-Optic Modulator or AOM. The light passes through the device and interacts with a transverse acoustic wave. The source frequency is upshifted or downshifted depending on the input acoustic frequency.

When a surface measurement is made an external ramp command is added to the vibration measurement and corrections made in the AOM. During the ramping an integrating bucket technique determines the phase for each point in the detector array. The phase map is determined and a surface map generated.

There are two nested phase shifting systems. The high frequency vibration compensation system described above uses phase shifts at a few kilo-Hertz to measure vibration. The low frequency surface measurement system initiates a ramp and uses an integrating bucket technique to generate surface maps. The high frequency system uses a single photodiode for vibration measurement and the low frequency system uses a CCD array for surface measurements. The rapid 2π shift isn't seen by the surface measurement system because the pixel intensities are integrated over 2π (EQN 1) Small errors are averaged over many cycles. The fringe contrast is reduced when the vibration servo is on.

$$\int_{\phi_0}^{\phi_0 + 2\cdot\pi} I(\phi)\, d\phi = \text{constant} \qquad \text{where: } \phi_o = \text{initial phase},\ I(\phi) = \text{intensity} \tag{1}$$

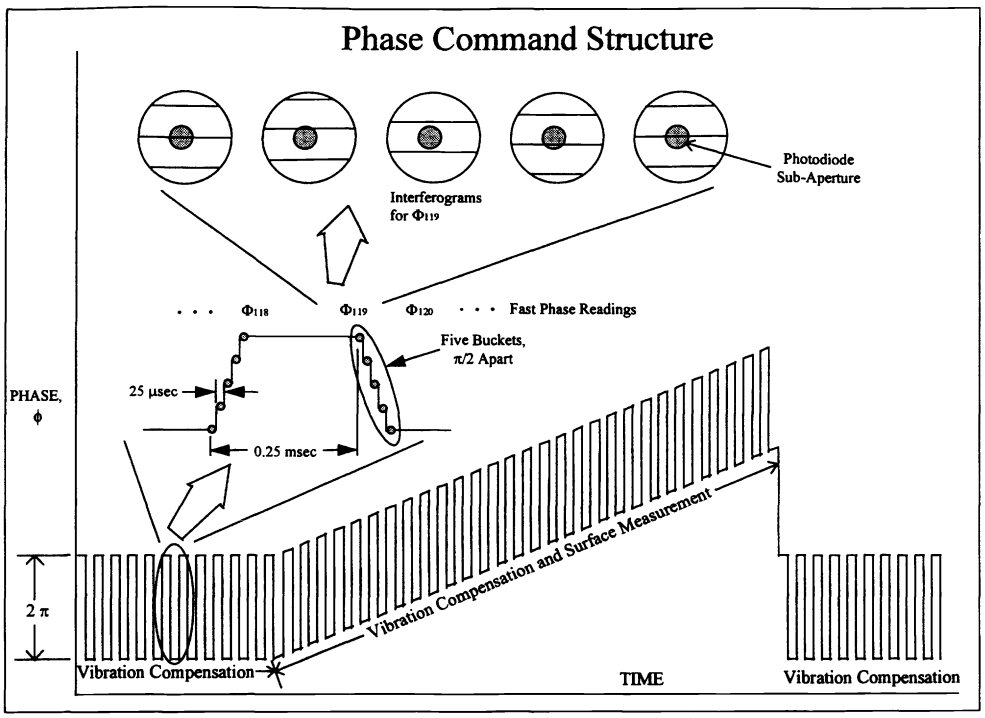

FIGURE 2. The basic phase command structure for the vibration compensation method. The photodiode intensities are used to calculate phase errors at 4000 Hertz. During a surface measurement, a ramp is initiated and an integrating bucket technique is used to calculate a phase map.

The proposed system installation is shown in Figure 3. Basically, the fixed frequency source is replaced with a source of controllable frequency. Light is split off and sent to a high speed photodiode where the voltages are used to make high speed phase measurements. The scheme accounts for optical path changes in piston which is the mode of primary significance.

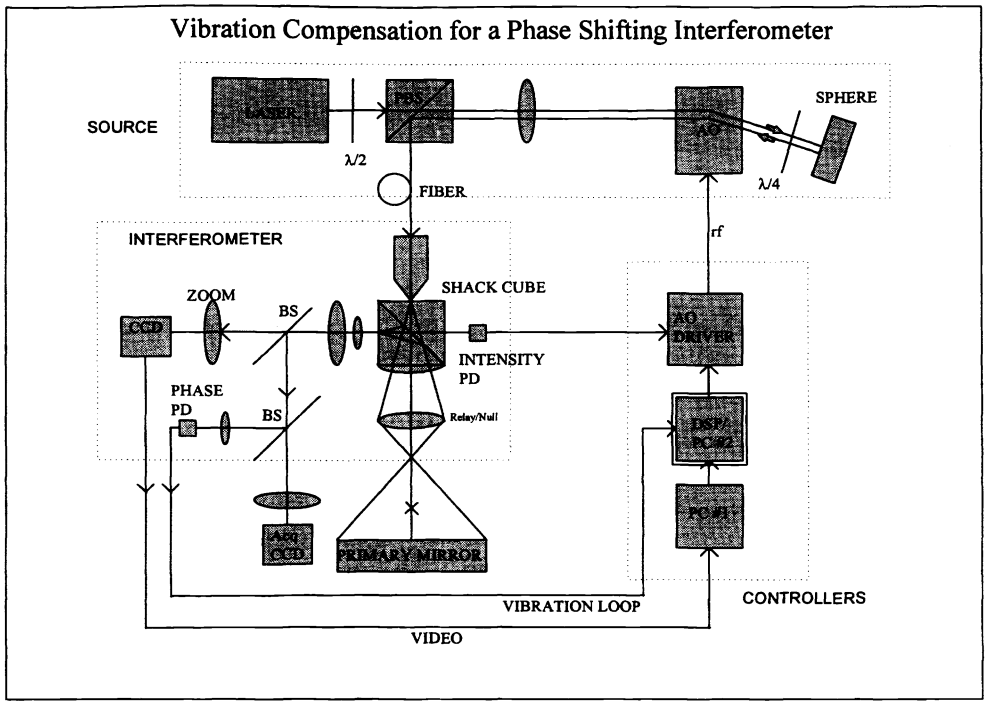

FIGURE 3. Installed System. This is a block diagram showing the key components for the interferometric testing of large primary mirrors. The vibration compensation and intensity loops are shown.

An interesting feature of the AOM implementation is shown in Figure 4. The angle at which the incident beam is diffracted in the AOM is dependent on the acoustic frequency. To avoid beam movement, a clever approach was devised. The source is focused onto the AOM where it is diffracted. The first order is allowed to pass and reflect off of the concave sphere. The sphere is positioned so that its center of curvature is coincident with the beam waist at the AOM. With this setup, as the beam moves on the sphere in response to acoustic frequency changes, the return beam always retraces the incident path. The net affect is that there is no beam movement and the beam remains efficiency coupled to the optical fiber. In addition, because the beam passes through the crystal twice, the frequency is shifted by twice as much.

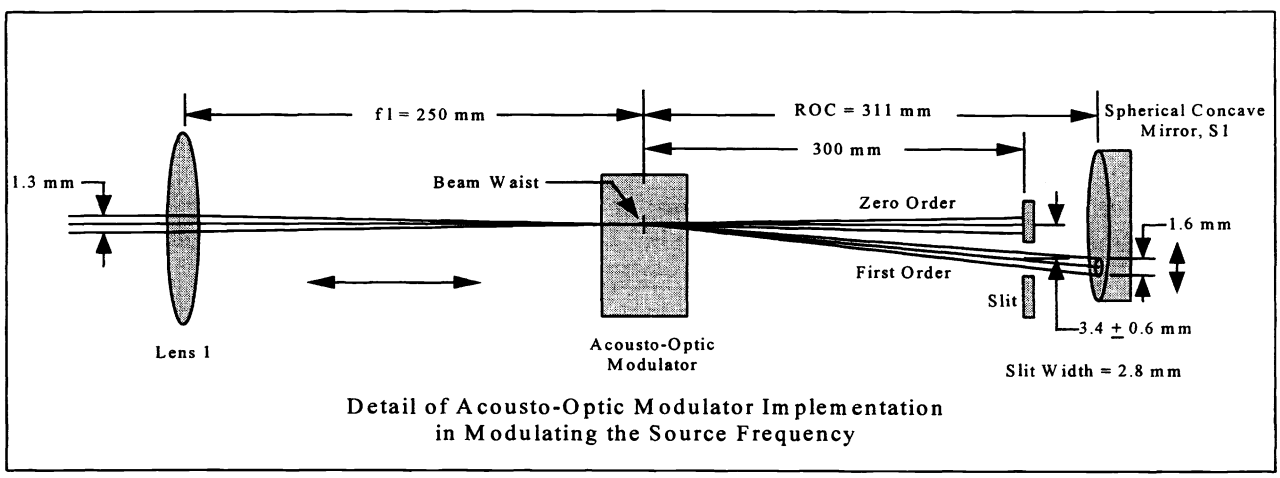

FIGURE 4. Detail of AOM implementation in controlling the source frequency. As the acoustic frequency is changed, the beam moves on the sphere but always retraces its path.

An integral part of the vibration compensation device is a DSP which takes real-time analog signals, converts them to digital, manipulates the data and finally reconstructs them in analog form. It is a dedicated and specialized processor programmed specifically for our needs. During normal operation the DSP sends commands to the AO driver to change the source frequency. If there is a positive phase change due to vibration, then the frequency is upshifted and vice versa. The specific features and subroutines of the code are described below. Note that the specific numbers used in the description can be easily changed within the DSP code to meet the needs of the operator. The calibration of the phase steps is controlled with the autocalibration subroutine.

Prior to a phase shifted surface measurement, the voltage from the outside PC (#1) is zero. When a surface measurement is made, the command voltage from PC #1 is ramped through several waves -- as required by the phase shift algorithm. During this surface measurement ramping, the fast phase measurement continues. The measurement command signal is added to the PC command and a correction made with the AO.

The layout of the lab experiment is shown in Figure 5 below. The test path of the test tower is duplicated by folding the path as shown. The path is folded 10 times between two mirrors with the fifth reflection off of a retro-reflecting corner cube. In this way, the test path is 34 meters -- the same as in the test tower for testing the MMT (Multiple Mirror Telescope) 6.5 meter mirror. The components have stiff mounts and natural frequencies well in excess of the frequencies of concern. The corner cube is PZT driven to provide a convenient, controllable vibration source. The corner cube can be driven with a variety of input waveforms, amplitudes and frequencies. In this way, the system performance can be optimized on the optical table prior to the installation in the test tower. Many of the system parameters can be adjusted within the DSP code.

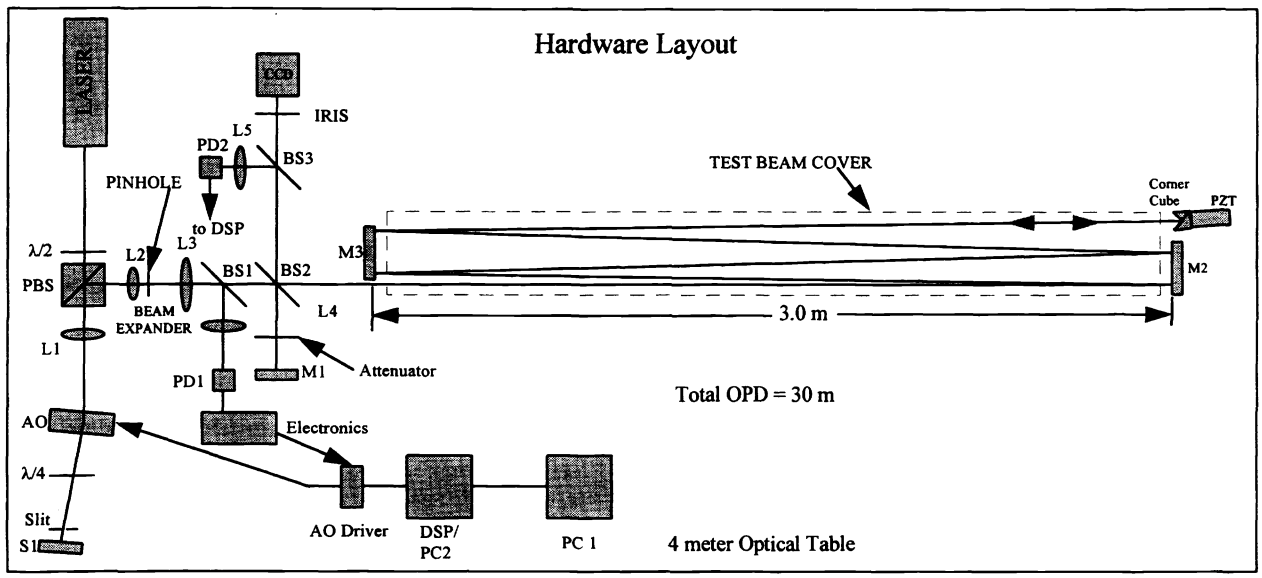

FIGURE 5. Hardware Layout. This diagram shows the layout of the hardware. A PZT driven corner cube acts as a vibration source and the system performance is measured.

3. RESULTS

Surface measurements give a true measure of the system performance. The RMS surface error versus frequency for various sample frequencies is given in Figure 6. All phase maps are surface maps and not wavefront maps. When data was taken, several phase maps were averaged for each point. In addition, the initial phase was slowly varied so that any errors

which were dependent on the initial phase were averaged to zero. The phase reduction software used was OptiCode / PCS, version 2.12 from Phase Shift Technologies.

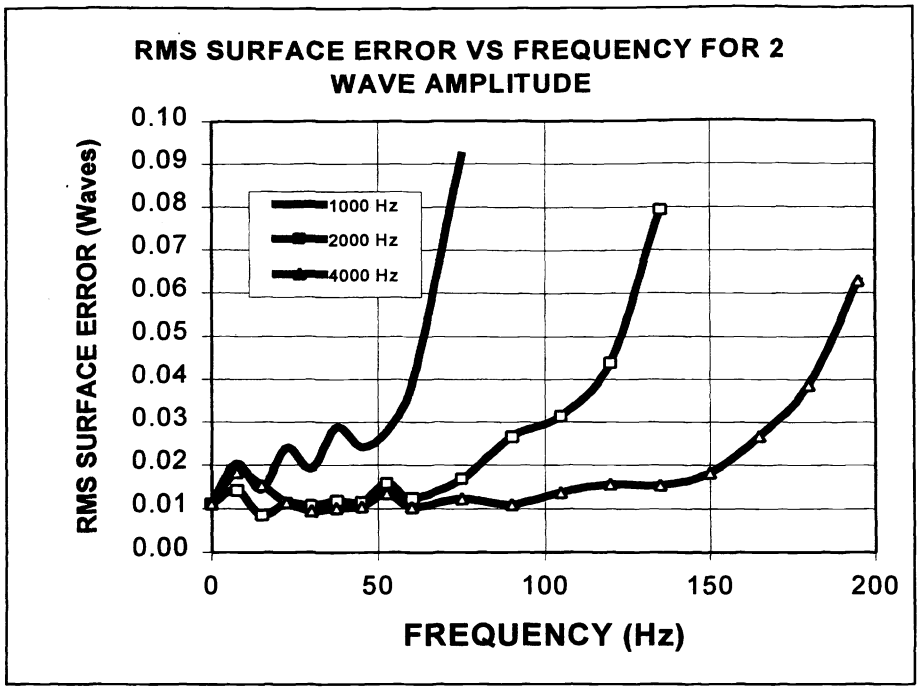

FIGURE 6. System performance for various phase sample frequencies. This indicates that the 4000 Hertz configuration has the advantage.

The system performance was mapped by comparing the RMS surface errors with the servo on and the servo off. The 4000 Hertz phase sample frequency was the best and was used for the rest of the system tests. Each data point results from the average of five phase maps. Frequencies from 0 to 200 Hertz were tested next and the data is given in Figure 7.

This data clearly shows the performance of the system and the advantage of its use. On average, for frequencies from 0 to 60 Hertz, the RMS surface error is reduced from 0.036 to 0.004 waves. There appears to be some residual influences even with the system on as can be seen by the small peaks at 15, 45 and 75 Hertz.

For most of the testing the vibrational input have been sinusoidal. This was a nice way to characterize the system but, real world inputs are typically more complicated and somewhat random. To test the system with a more realistic input, an ordinary household blender was set on the optical table and run during testing. To further test the device, frozen banana chunks were added during surface measurements. The vibration compensation device did an excellent job in reducing the RMS surface error as can be seen by Figure 8.

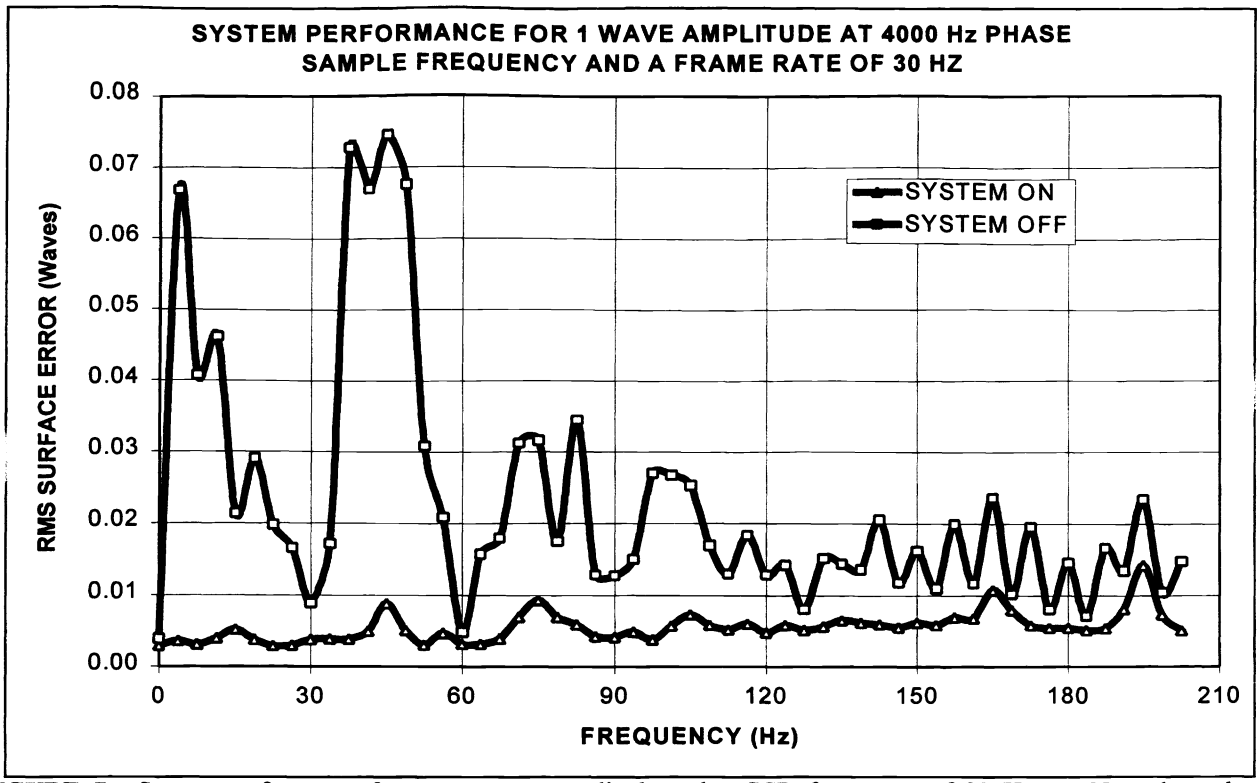

FIGURE 7. System performance for a one wave amplitude and a CCD frame rate of 30 Hertz. Note the reduced sensitivities at 30 and 60 Hertz.

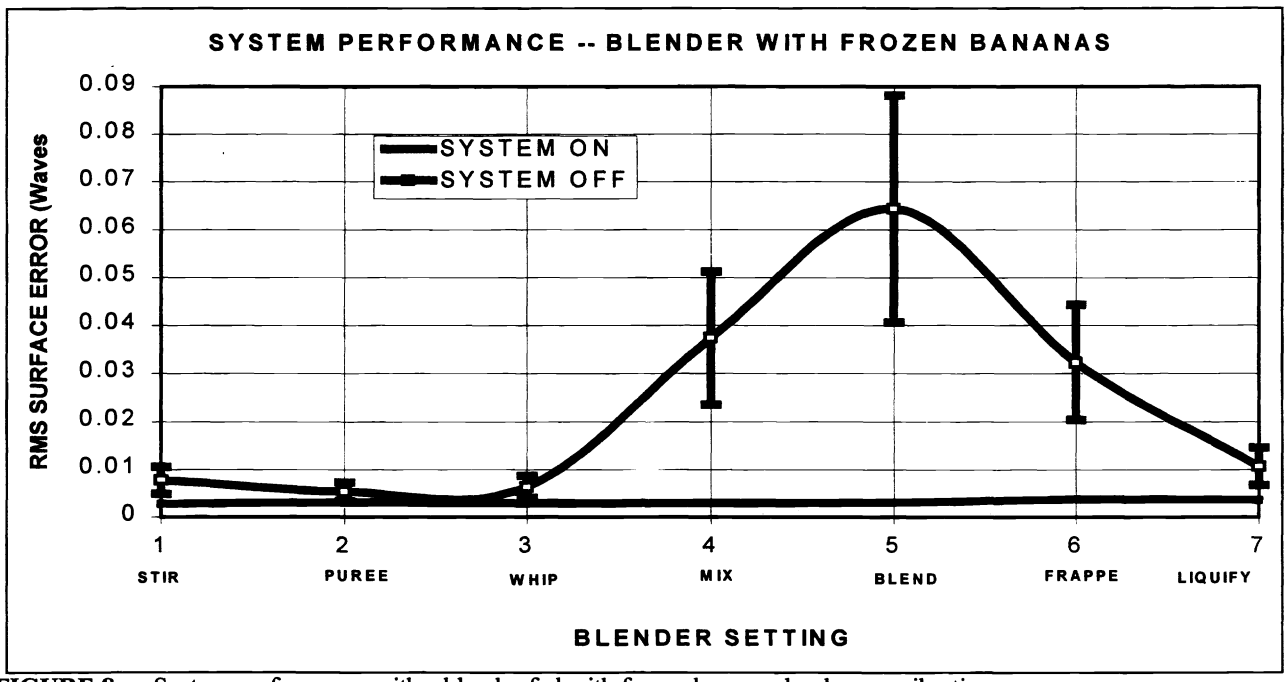

FIGURE 8. System performance with a blender fed with frozen banana chunks as a vibration source.

4. IMPROVEMENTS

The current implementation of the device corrects only the piston mode of vibration. In other words, the only direction of vibration that is compensated for lies in the direction of the optical axis. This is the mode of primary significance and observation of active test fringes corroborates this.

An improvement would be to include tip and tilt in addition to piston. To do this, we must add some complexity to the design. The approach involves adding two more active sub-aperture detectors. The AOM modulates the source frequency for the high frequency phase measurements and each of the three zones is looked at separately. For a Twymann-Green interferometer, this information is used in combination with 3 PZT's mounted to the reference mirror to compensate for tip, tilt and piston. For a Fizeau type of interferometer (like the Shack cube interferometer) the 3 PZTs can be used to move the reference surface in tip, tilt and piston. There is some frequency bandwidth limitation due to the dynamic response of the system.

With the current design, a change in the OPD is compensated for with a change in the source frequency. This is achieved through the use of an AOM. But the AOM is limited to a bandwidth of 80 $\pm$ 30 MHz. For the test path length of 34 meters this yields a maximum vibration amplitude of 7 waves that can be compensated. For the long test paths intrinsic to large telescope primaries, this is fine. But for the majority of phase shifting interferometers, the path difference between the test and reference arms is much shorter -- perhaps millimeters rather than meters.

For the device to be a useful addition or upgrade to existing interferometers, it must be able to compensate for short optical path lengths. One approach is to enhance the existing design and replace the AOM with an Electro-Optic Modulator (EOM). The EOM could be placed in the reference arm of a Twymann-Green interferometer (see Figure 9). The phase in the reference arm could be modulated as the active compensating element. These modulators have a better response time than the AOM but more importantly, the phase modulation (rather than frequency modulation) would be useful even with very short path lengths.

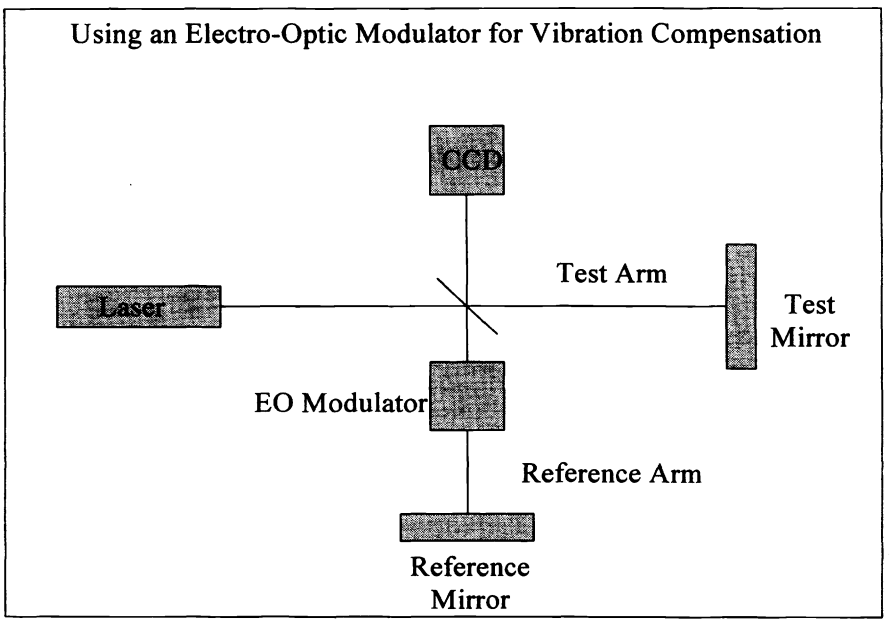

FIGURE 9. Using an EOM in the reference arm of a Twymann-Green interferometer allows for vibration compensation for short path lengths.

5. CONCLUSIONS

The vibration compensation device did a good job in reducing the RMS surface errors and is useful for long path length interferometry in bad environments. The system can significantly reduce the vibration errors or in some cases make testing possible where the normal phase shift system fails. The basic principle of the device has proven its efficacy and is not limited to long path applications. The addition an EOM in the reference arm would be useful for much shorter path lengths and could be implemented into many existing interferometers.

ACKNOWLEDGEMENT

The vibration compensation device was the masters thesis project for Glen Cole and was supported by the Steward Observatory Mirror Lab at the University of Arizona in Tucson, Arizona.

REFERENCES

1. Bateman, A., and Yates, W., *Digital Signal Processing Design,* (Computer Science Press, 1989).
2. Burge, J. H., *Advanced techniques for measuring primary mirrors for astronomical telescopes*, Ph. D. Dissertation, Optical Sciences, University of Arizona (1993).
3. Burge, J. H., Anderson, D. S., Ketelsen, D. A., West, S. C., "Null test optics for the MMT and Magellan 6.5-m *f*/1.25 primary mirrors," in *Advanced Technology Optical Telescopes V,* L. M. Stepp, Editor, Proc. SPIE **2199**, 658 - 669, (1994).
4. Cheng, Y., Wyant, J., "Phase shifter calibration in phase-shifting interferometry," Appl. Opt. **24**, pp. 3049-3052 (1985).
5. Creath, K., "Phase-measurement interferometry techniques," in *Progress in Optics* **26**, E. Wolf, Editor (Elsevier, New York, 1988) pp. 349-393.
6. Deck, L., "Vibration-resistant phase-shifting interferometry," Appl. Opt. **35**, pp. 6655-6662 (1996).
7. de Groot, P. J., Deck, L. L., "Numerical simulations of vibration in phase-shifting interferometry," Appl. Opt. **35**, 2172-2178 (1996).
8. Greivenkamp, J. E., "Sub-Nyquist interferometry," Appl. Opt. **26**, 5245 - 5228 (1987).
9. Greivenkamp, J. E. and J. H. Bruning, "Phase Shifting Interferometry," in *Optical Shop Testing*, D. Malacara, Editor (Wiley, New York, 1992) pp. 501-598.
10. Hull, C., Siegmund, W., "Steward Observatory Mirror Laboratory Test Tower: Vibration Study," University of Washington (1992).
11. Koliopoulos, C. L., "Simultaneous phase shift interferometer," in *Advanced Optical Manufacturing and Testing II,* Proc. SPIE **1531**, pp. 119-127 (1991).
12. MacQuigg, D. R."Hologram fringe stabilization method," Appl. Opt. **16**, pp. 291-292 (1977).
13. Malacara, D. and S.L. DeVore, "Interferogram Evaluation and Wavefront Fitting," in *Optical Shop Testing*, D. Malacara, Editor, (Wiley, New York, 1992) pp. 455-499.
14. Neumann, D. B., Rose, H. W., "Improvement of recorded holographic fringes by feedback control," Appl. Opt. **6**, pp. 1097-1104 (1967).
15. Sasaki, O., Takahashi, K., Suzuki, T., "Sinusoidal phase modulating laser diode interferometer with a feedback control system to eliminate external disturbance," Opt. Eng. **29**, pp.1511-1515 (1990).
16. Shack, R. V. and G. W. Hopkins, The Shack interferometer," Opt. Eng. **18**, 226-228 (1979).
17. Weiman, C. E., Hollberg, L., "Using diode lasers for atomic physics," *Rev. Sci. Instrum.,* 62(1), (1991).
18. Wyant, J. C., Course notes from "Optical Testing and Testing Instrumentation," Optical Sciences 513, University of Arizona (1995).
19. Yamaguchi, I., Liu, J., Kato, J, "Active phase-shifting interferometers for shape and deformation measurements," Opt. Eng. **35**, pp. 2930-2937 (1996).